

Thin crust as evidence for depleted mantle supporting the Marion Rise

Huaiyang Zhou¹ & Henry J. B. Dick²

The global ridge system is dominated by oceanic rises reflecting large variations in axial depth associated with mantle hotspots. The little-studied Marion Rise is as large as the Icelandic Rise, considering both length and depth, but has an axial rift (rather than a high) nearly its entire length. Uniquely along the Southwest Indian Ridge systematic sampling allows direct examination of crustal architecture over its full length. Here we show that, unlike the Icelandic Rise, peridotites are extensively exposed high on the rise, revealing that the crust is generally thin, and often missing, over a rifted rise. Therefore the Marion Rise must be largely an isostatic response to ancient melting events that created low-density depleted mantle beneath the Southwest Indian Ridge rather than thickened crust or a large thermal anomaly. The origin of this depleted mantle is probably the mantle emplaced into the African asthenosphere during the Karoo and Madagascar flood basalt events.

Following Morgan¹, oceanic rises are thought to form via a hot fertile mantle plume producing a flow of plume-derived mantle to the ridge and down the subaxial asthenospheric channel, resulting in increased mantle temperature, ridge topography, and thickened igneous crust; this is the mantle wedge hypothesis (see ref. 2 for example). Studies of the Reykjanes ridge support this, with seismic crust thickening from about 6 km near the Gibbs fracture zone for 1,600 km to about 18 km at the Reykjanes peninsula, for example³. The Icelandic rise also has a long axial high consistent with such robust magmatism⁴ (Table 1). The current consensus is that the igneous crust thickens over the Marion Rise, and indeed up all rises^{5,6}. The basalt sodium contents, as at other rises, decrease systematically with proximity to the Marion hotspot, and are interpreted to represent higher degrees of mantle melting and thicker crust⁷. Such correlations, however, can be due to variable mantle temperature or to an increasingly depleted mantle source composition, and do not require thicker crust⁸. The Marion Rise, in particular, has numerous large-offset transforms that would block subaxial asthenospheric flow⁹, and its deep rift valley indicates weak rather than robust magmatism⁴. Niu and O'Hara¹⁰, although assuming thick crust over rises, suggest that the global correlation of basalt chemistry and ridge depth is best explained by mantle

composition variations, with many rises supported by depleted chemically buoyant mantle, as for the Iceland¹¹ and Azores¹² rises.

The only available seismic data predicts 2–6 km of crust in the Southwest Indian Ridge (SWIR) rift mountains at 57° E and 61° E (ref. 13). Modelling using sea surface gravity gives 2–4 km in the eastern SWIR, but around 6–12 km north of Marion Island¹⁴. Given that mantle peridotites are locally abundantly exposed, however, 6–12 km of igneous crust seems unlikely in the latter region. Muller *et al.*¹⁵ found the Mohorovičić discontinuity (the Moho) 5 ± 1 km beneath the Atlantis Bank at 57° E, but concluded that it could be a serpentinization front. Similarly, the seismic determination of crustal thickness at 61° E is at odds with mapping east of the Melville fracture zone that shows the ridge to consist of local magmatic centres linked by nearly amagmatic oblique segments producing “smooth” sea floor¹⁶. Hence, the equivalency of seismic and igneous ‘crust’ is not established for slow- and ultraslow-spreading ridges¹⁷.

All estimates of ocean crust thickness are by inference from geochemistry, seismic data and gravity. Nowhere have they been tested by direct geologic constraints, which would require deep-ocean drilling. Mapping and sampling in lower crust and mantle exposed in oceanic core complexes, however, can constrain crustal thickness^{18,19}. Using

Table 1 | Characteristics of rifted and axial rises

Rise	Dominant morphology	Spreading rate (mm yr ⁻¹)	Hotspot magma flux (m ³ s ⁻¹)	Crustal volume (10 ⁷ km ³)	Elevation range, minimum to maximum (m)	200-km-average elevation range (m)	Depth anomaly (m)	Rise length (km)	Cross-sectional area (km ²)	Geographic location
Iceland	Axial high	19.5	7.0	4.53 (ref. 5)	750, -3,115	642, -2,425	3,067	2,390	3,665,156	Jan Mayen to Gibbs fracture zone at 53° S
Galapagos	Axial high	63.0	5.5 (ref. 6)	NA	-1,361, -3,732	-1,762, -3,170	1,408	1,380	970,988	Cocos-Nazca Rise 85.2°–97.5° W
Azores	Axial rift	20.5	NA	1.15 (ref. 5)	-345, -4,127	-1,659, -3,441	1,782	2,877	2,563,557	MAR 47.5°–25.8° N
Marion	Axial rift	14.6	0.4 (ref. 14)	0.95 (ref. 14)	-858, -5,150	-2,547, -4,681	2,134	3,408	3,636,236	SWIR 32.32°–63.34° E

NA, not available. The maximum and minimum elevation is measured at the lowest and the highest topographic point on each rise. These points are defined by the midpoints of the rift-valley axis where the smoothed ridge depth stops decreasing or increasing. The 200-km average maximum and minimum elevations represent 200-km along-axis average depths taken about these points to eliminate local topographic effects. The depth anomaly is computed from the average depths. Cross-sectional area is simply an estimate of size of the rise based on half its length times its total depth anomaly, which shows that the Iceland and Marion rises, in these terms, are approximately the same size.

¹State Key Laboratory of Marine Geology, Tongji University, Shanghai, 200092, China. ²Woods Hole Oceanographic Institution, Woods Hole, Massachusetts 02543, USA.

this approach, H.Z. surveyed a ridge segment at 53° E where low-basalt Na_8 (ref. 20; Na_8 is the Na content of basalt corrected for fractional crystallization), refractory peridotite, gravity¹⁴, and the mantle wedge hypothesis suggested that 4–8 km of crust might be present. Instead of thick crust, however, H.Z. found nearly amagmatic spreading, supporting our interpretation of sampling elsewhere on the ridge.

Tectonic setting

The SWIR is a highly oblique ultraslow-spreading ridge with a near-constant full rate of approximately 14 mm yr^{-1} (ref. 21), extending 7,700 km between the Bouvet and Rodriguez triple junctions (Fig. 1). East of the Bouvet triple junction at 25° E it is abruptly offset about 1,800 km to the northeast by the DuToit, Andrew Bain, Marion, and Prince Edward fracture zones²². There it crosses the flank of the Southern Ocean geoid high, following a subdued positive arch over the Marion swell from the Andrew Bain fracture zone to the Gallieni fracture zone. The Marion Rise extends for around 3,400 km, starting at a depth of 4,800 m at 27° E before rising abruptly to a depth of 858 m at 36° E, and then down to 5,150 m at 63° E.

A 1.5-km-high and 70-km-long axial volcano at 36° E forms a short axial ridge marking the maximum volcanic activity on the rise. This is attributed to flow of plume-derived mantle to the ridge from beneath the Marion hotspot 256 km to the south²³. Gravity, however, indicates that any influence of the Marion hotspot is limited to west of the Discovery II fracture zone^{9,24}. Except for the 36° E segment, the entire SWIR has a deep axial rift. The SWIR east of the Indomed fracture zone formed by propagation of the Rodriguez triple junction over the last 64 million years²¹. It has regularly spaced non-transform discontinuities, short oblique amagmatic segments, and the Atlantis II, Novara, and Melville transforms.

Geology

Figure 1 shows a compilation of satellite-navigated dredges (Supplementary Table 1), with which we interpreted crustal architecture along the SWIR (see Methods). Peridotite and gabbro are widely distributed over the entire ridge, although most dredging focused

on rift-valley neovolcanic zones. This severely biased recoveries to basalt, as even a thin lava veneer prevents the sampling of plutonic rock. Dredges on rift-valley walls, non-transform discontinuities, and transforms are comparatively few, except along the western SWIR and the Atlantis II fracture zone. From 9°–35° E and 41°–47° E (ref. 25) peridotite is abundant, demonstrating thin or missing basaltic crust and enormous mantle exposures^{25–27}. Despite its frequent occurrence, however, gabbro is volumetrically scarce, and, excluding the Atlantis II fracture zone (Fig. 2b), accounts for less than 11% of the plutonic rocks dredged along the SWIR (Fig. 2a). Thus, while gabbro and peridotite occur in 25 dredges at 9°–16° E, there is 1,570 kg of peridotite but only 49 kg of gabbro. With only scattered basalt flows dredged in the rift valley, this is essentially a 400-km-long ‘amagmatic’ segment²⁸. Similarly, although there are 21 peridotite-bearing and 17 gabbro-bearing Scripps Protea Expedition dredges from 31°–39° E, they recovered 3,451 kg of peridotite, and only 799 kg of gabbro.

Most SWIR peridotites are partially serpentinized (20%–70%) statically altered granular rocks with fine serpentine vein networks (Supplementary Figs 1 and 2). They have protogranular texture with smooth, curved grain boundaries interlocking with olivine, or an overprinting porphyroclastic texture due to high-temperature crystal-plastic deformation. Associated mylonites, which constitute around 5% of abyssal peridotites²⁹, reflect extreme deformation produced by strain localization, with olivine–spinel geothermometry indicating closure temperatures of about 600–750 °C (ref. 30). Hydrothermally altered and sheared talc–serpentine and talc–tremolite schist represent less than 10% of the peridotites. These assemblages reflect progressive strain localization from high-temperature crystal-plastic deformation (at over 1,000 °C), followed by mylonite formation, to low-temperature brittle faulting accompanying unroofing and final emplacement to the sea floor^{19,31}.

The 53° E amagmatic segment

In 2010 the RV *Dayang Yihao* mapped approximately 11,000 km² between the Gallieni and Gauss fracture zones (Fig. 3). This comprised a ridge segment with a deep rift valley with 2.4-km relief at

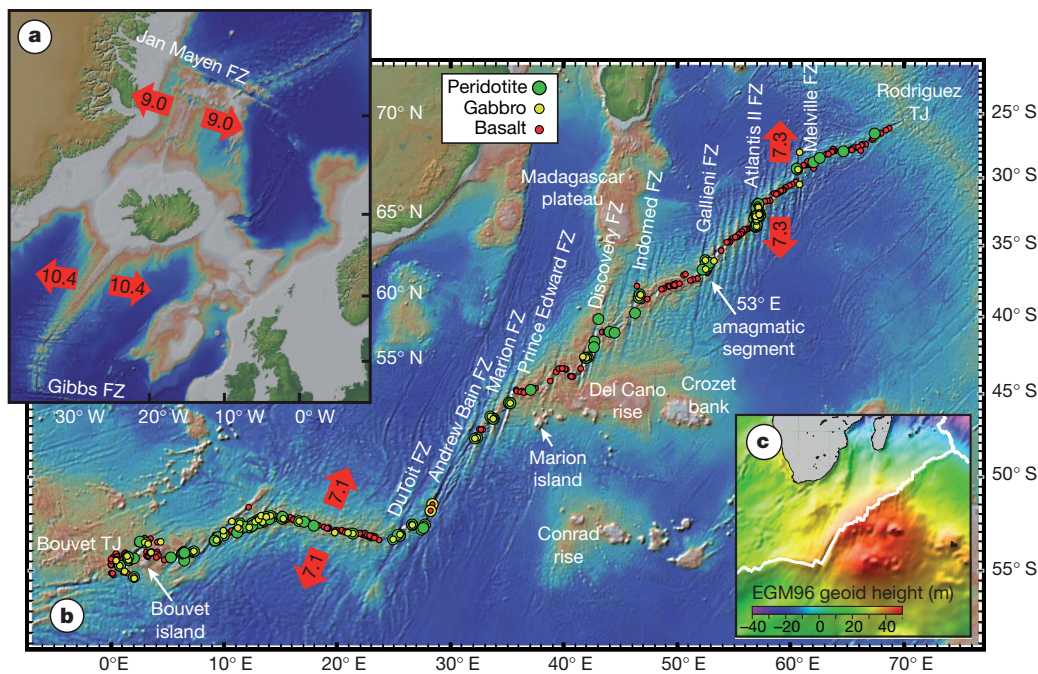


Figure 1 | Physiographic and geoid maps of the SWIR with sample locations, and a map of the Icelandic rise for comparison. Spreading directions and half rates are given in millimeters on the red arrows. **a**, Relief map of the Icelandic swell. **b**, Map of the Marion swell with location of satellite-navigated dredges on the SWIR. **c**, Free-air geoid map showing the position of

the SWIR (courtesy of Mark Behn). EGM96 is Earth Gravitational Model 1996. Maps of the SWIR and Icelandic Rise plotted at the same scale for comparison. (www.geomapp.org). Spreading rates were calculated using the global plate velocity model Nuvel 1. Symbol sizes are not proportional to recovery. Data and sources are given in Supplementary Table 1. FZ, fracture zone; TJ, triple junction.

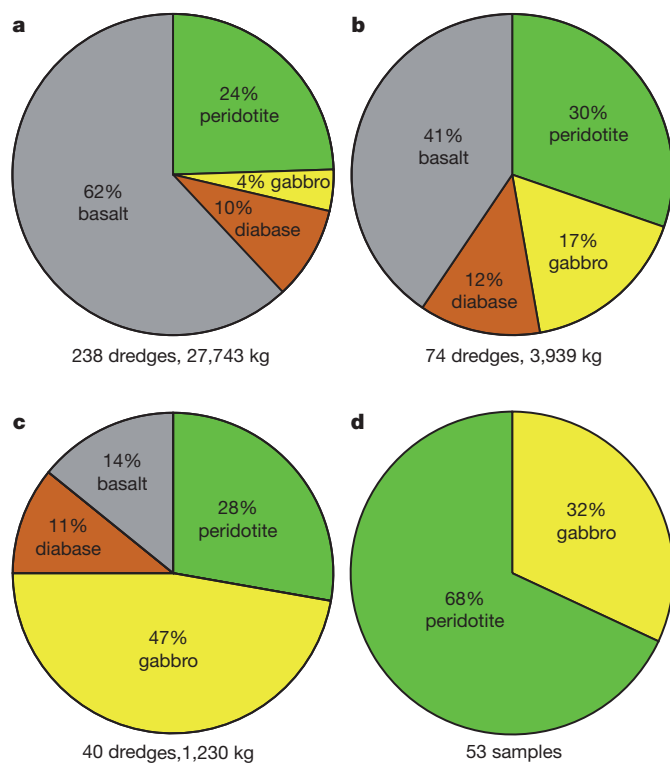


Figure 2 | Lithologic proportions by weight for SWIR dredges compiled from Supplementary Table 1 with proportions for the MAR Atlantis massif. **a**, SWIR excluding the Atlantis II fracture zone at 57° E. **b**, Atlantis II fracture zone including the Atlantis Bank. **c**, Atlantis Bank excluding the rest of the Atlantis II fracture zone (32.5–33° S). **d**, The Atlantis massif, MAR, with lithologic proportions by number of dive samples collected on the flanking transform wall, compiled from ref. 47. The transform gabbros are interpreted as a precursor net-vein complex intruded into massive granular peridotite from the 1,400-m gabbro sequence drilled 4.5 km to the north at Integrated Ocean Drilling Program Hole U1309D.

its midpoint, plunging from a water depth of 3.9 km to over 5 km at the 107-km-offset Gallieni fracture zone. The rift valley lacks an axial high, and is bowed north at its centre. Eleven dredges and three television-guided (TV) grabs (which spot-sample the sea floor) collected about 1,938 kg of rock (Supplementary Table 2). The Scripps Institution of Oceanography Indomed Expedition Leg 8 sampled peridotite (dredge 12) and basalt (dredge 15) from the western Gallieni Transform wall, and basalt low on the eastern wall (dredge 13), while the RV *Marion Dufresne* Edul Cruise Leg 107 dredged 2 kg of dunite and 20 kg of basalt from the rift-valley centre (dredge 69).

RV *Dayang Yihao* recovered 422 kg of basaltic rock. Diabase occurred with peridotite in dredges 6 and 8, with a small gabbro xenolith in one diabase. The remaining basalts are fine-grained to very-fine-grained, some with pillow rinds and one with glass. They are heavily weathered, but hydrothermally unaltered. Where associated with peridotite outcrops, they are probably hanging-wall debris rafted on fault footwalls. A 250-kg gabbro block from the eastern inside-corner high and seafloor physiography indicates a possible 380-km² gabbroic core complex there, consistent with volcanic crust indicated by the east-west lineated terrain in the eastern rift mountains.

Peridotite is extensively exposed in the western half of the segment and to the north and south in the rift mountains flanking the Gallieni fracture zone. The western outside-corner high lacks well developed ridge-parallel lineations, consisting instead of small domes where 204 kg of serpentinized peridotite and a small amount of gabbro were dredged. Seven stations in the southern rift mountains recovered around 1,062 kg, mostly harzburgite. Three *en echelon* domed ridges, progressively staggered to the north from the transform to the segment

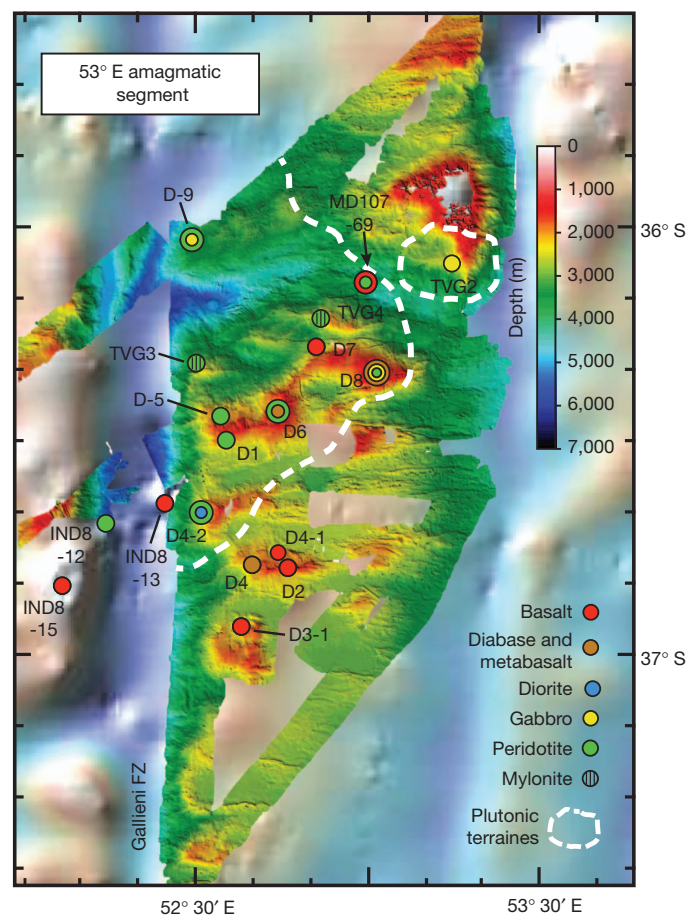


Figure 3 | Bathymetric map of the 53° E ridge amagmatic segment with sample locations and contents. The Simrad EM120 multi-beam map covers around 11,000 km² embedded in the sea surface gravity map from GeoMapApp (www.geomapp.org). Filled circles indicate dredge and TV grab locations. Multiple lithologies are indicated by nested symbols, with smaller insets representing the volumetrically lesser rock type. D and TVG prefixes represent the RV *Dayang Yihao* cruise 21 samples; IND indicates the Scripps Institution of Oceanography Indomed Expedition Leg 8; MD107 indicates the RV *Marion Dufresne* Cruise 107 samples. Dashed white lines outline areas of probable massive exposure of peridotite (around 3,200 km², western area) and gabbro (around 380 km², eastern area) interpolated using seafloor morphologies. The colour scale gives depth in metres.

centre, flank the western rift valley. They are about 8–11 km wide and 20–28 km long, shoaling to 1,000–2,800 m depth, with the largest emerging from the centre of the rift valley. TV grabs from the eastern and westernmost domed ridges recovered serpentinized granular and mylonite peridotite. Immediately south of the easternmost, dredge 8 recovered diabase, gabbro and serpentinite from a large 28 km × 13 km north–south corrugated dome. Further southwest at about 36° 28' S, peridotite was dredged at three locations on another irregular ~20 km × 35 km domed region with evidence of north–south corrugations. Peridotite with a diorite fragment was found on the transform wall at the end of an east–west ridge at approximately 36° 40' S (dredge D4-2). Outside these mantle exposures, only basalt was dredged to the southeast of D4-2, defining the limits of the mantle outcrops. The peridotite exposure flanking the Gallieni transform, then, is about 110 km in the spreading direction and up to 60 km wide, or about 3,200 km²—probably much bigger if the peridotite outcrops extend further north.

Compared to other large fracture zones, the uplift at the western inside-corner high is modest, composed of the three small axis-parallel domes, rather than one large dome, similar to those found on the opposing outside-corner high. These are distinct from more regularly lineated terrains characteristic of rifted volcanic crust in the eastern rift

mountains. Such terrain is also inconsistent with the asymmetric detachment faulting seen at large oceanic core complexes. Rather, it is generally associated with block faults exposing massive peridotite at amagmatic ridge segments¹⁶. The broader domes sampled by dredges 1, 5, 6 and 8, however, feature corrugations and some mixed lithologies characteristic of oceanic core complexes. Bathymetry and dredging, then, indicate a progressive eastward transformation from magmatic to amagmatic spreading from about 9.4 million years ago to the present in the western portion of the 53° E segment (assuming symmetric spreading), with the formation of core complexes followed by more symmetric block faulting exposing an enormous region of partially serpentinized peridotite.

Spinel in 16 peridotites from seven stations from the rift mountains and eastern Gallieni fracture-zone wall (Supplementary Table 3) and ten peridotites from two stations from the western wall (H.J.B.D., personal communication) have average spinel $\text{Cr} \times 100 / (\text{Cr} + \text{Al}) \approx 30$ corresponding to about 12% average melting³² of a hypothetical primitive upper-mantle composition³⁵. A basalt glass fragment from the 53° E segment has Na_8 of 2.8; whereas those from the ridge to the east and west have average Na_8 of 2.5, predicting around 4–6 km of crust and a ridge depth of around 2,500 m (ref. 20)—which is 1,000 m shallower than what is actually observed.

Crustal architecture

Abyssal peridotites have three principal emplacement modes, each with characteristic unique textures, distribution, and associations (see Methods). These include diapiric emplacement of highly sheared talc–serpentine schists and serpentinites along both low- and high-angle faults cutting laterally or vertically through the crust into peridotite. Texturally, however, most abyssal peridotites are typical of those in large ophiolite peridotite massifs. Consistent with this, 65 of 119 SWIR peridotite dredges recovered no gabbro, and many of the rest only gabbro veins. A typical dredge covers 500–1,000 m, and multiple dredges often find little but peridotite in an area. A detachment fault exposing mantle peridotite from beneath 4–8 km of gabbro and basalt requires many kilometres of throw and heave, and gabbroic hanging-wall debris should be scattered over the fault surface along with pillow lava and diabase. There would also be gabbro inliers in the footwall owing to fault imbrication.

Where ocean drilling or mapping has found massive gabbro, as at the Atlantis Bank and the Atlantis massif, it is extensively exposed intruding peridotite on the transform wall (Fig. 2c, d). Similarly, at 23° N on the Mid-Atlantic Ridge (MAR) gabbro complexes intruded into mantle peridotite were mapped by dredging³⁴ and then confirmed and extended by seismic refraction³⁵. A series of Ocean Drilling Program (ODP) holes in MAR tectonic windows at 14°–16° N (ref. 36) also confirm a ‘plum pudding’ model of gabbro intrusions in serpentinized mantle³⁷ constructed from bathymetry, dredging and diving. In these holes abundant gabbro veins and dikes were consistent precursors of larger gabbro bodies. The numerous gabbro veins and intrusions in peridotite on the transform wall of the Atlantis massif (Fig. 2d) then suggested the presence of the over-1,400-m gabbro body later drilled a few kilometres to the north. In all these cases, gabbro is far more abundant than it is generally along the SWIR. Moreover, gabbroic core complexes, such as the Atlantis Bank³⁸, the Atlantis massif¹⁸, the Kane Megamullion¹⁹, and 23° S (ref. 39) all show that where gabbroic crust is present, detachment faults root there, not in the mantle. Thus, on the basis of rock textures and distribution, the SWIR peridotite localities mainly represent massive partially serpentinized mantle exposed over large seafloor regions.

Thus sampling shows thin or missing crust over the Marion Rise. Although peridotite is exposed on transform walls by detachment faulting rooted through the nearby dike–gabbro transition, as at the Atlantis II fracture zone, in most areas the associated gabbro bodies had to be very small. Many peridotite exposures, as at 53° E, are due to amagmatic spreading. Where gabbro is largely missing, the crust is

probably limited to <1–2 km, based on the known depths of the dike–gabbro transition, and hence the conductive–advective heat flow transition beneath ridges⁴⁰ (cooling is too rapid for gabbro to form in the advective cooling regime). In rare areas, as at Atlantis Bank, where gabbro is abundant, the crust may be over 4 km thick¹⁸, whereas in regions where largely mantle is exposed it may be largely missing. With this degree of lateral heterogeneity a precise estimate of average crustal thickness is difficult. It is possible that in the eastern SWIR, where ‘smooth’ sea floor indicative of block and detachment faulting predominates⁴¹, the average crust could be as little as 1 km, and that over the Marion swell, where regions with more igneous crust may occur, the average crust could be about 2 km. But geologically, there is not nearly enough crust along the ridge to explain the formation of the Marion Rise using any model that precludes mantle compositional buoyancy as the major contributor.

Discussion

The numerous exposures of mantle peridotite and sparsity of gabbro over the Marion Rise overturns the iconic model that rises are all characterized by thick crust. This confirms the hypothesis that ocean rises can be supported by highly depleted buoyant mantle. Opposing models with uniform mantle composition and large variations in mantle potential temperature require correspondingly large variations in crustal thickness²⁰. Differences between rifted and axial rises also cannot be attributed to spreading rate, as this is virtually uniform along the Marion Rise, and varies little up the Iceland and Azores rises, whereas the spreading rates of the rifted Marion and Azores rises bracket that of the axial Icelandic rise (Table 1).

Without a large flux of hot primitive mantle or thick crust, a rifted rise can be supported by a thermal or compositional anomaly. For the latter case, Niu and O’Hara¹⁰ analysed global ridge-depth variability but found no convincing evidence for ridge temperature gradients exceeding 50°–100° K (ref. 10). They point out, however, that below about 70 km in the garnet peridotite facies, the density difference between fertile garnet lherzolite and depleted harzburgite is very large^{10–12,42}—as much as 1.2%. Consistent with the large compositional variation of abyssal peridotites⁸, a 0.6% density contrast can easily account for the global ridge-depth variation, requiring compensation down to 458 km. Proportionately then, the local 2.1-km Marion Rise depth anomaly could be compensated in the upper 200–250 km entirely in the asthenosphere. Even assuming large temperature anomalies, however, it has been noted⁴³ that the Hawaiian swell, possibly the largest thermal plume on the planet, has a peak amplitude of only about 1.4 km. Similarly, Ito *et al.*⁴⁴ found that only 1.3 km of their predicted 3.7-km Icelandic topographic anomaly could be supported by a 180 °C mantle temperature anomaly, the rest being an isostatic response to crustal thickness. Thus, it is very unlikely that the geriatric Marion plume could account for the 2.1-km depth anomaly along the Marion Rise.

Mantle composition gradients along rises can explain their gravity signal, which, when modelled assuming uniform mantle composition, predicts 8–10 km of crust on the Marion and Azores rises^{14,45}. Varying serpentinization depth is not a likely alternative because serpentine is unlikely to be stable to a depth of 9–10 km beneath a ridge. Models for the Moho as a serpentinization front attribute this to tectonic uplift into the rift mountains as the lithosphere cools into the serpentine stability field⁴⁶. Where the Moho is probably a serpentinization front at the Gakkal ridge, the seismic crust is only 1.9–3.3 km thick¹⁷. Such a front is controlled by the thermal structure at the ridge axis, and if anything, its contribution to the depth anomaly should be negative if mantle temperature and crustal thickness increase towards the high.

We have shown that a large region of previously depleted mantle supports the Marion Rise rather than down-axis intrusion of hot primitive mantle (Fig. 4). Thin crust requires this explanation, because any thermal anomaly requires a more refractory mantle to offset the accompanying increase in melting. Without an enormous

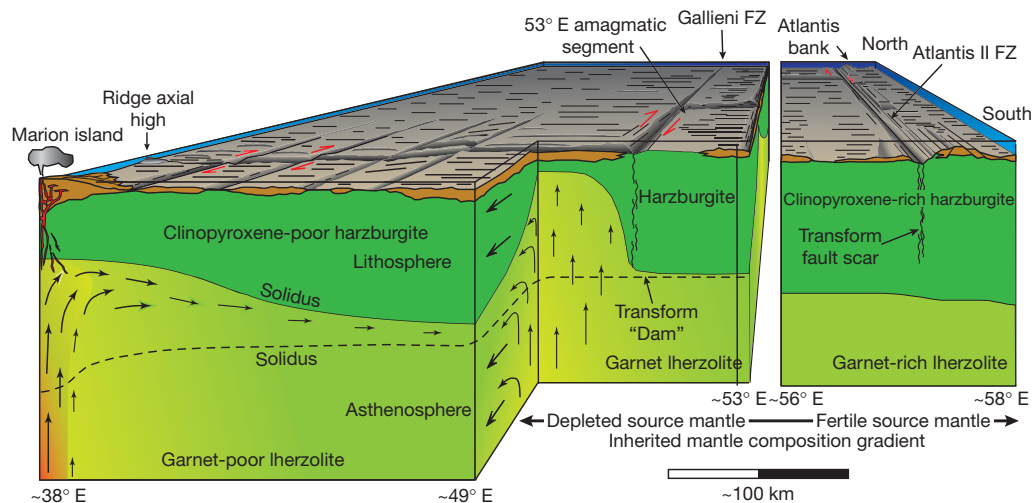


Figure 4 | Cartoon looking north from the Antarctic plate across the SWIR, showing the inferred crustal architecture along the Marion Rise. Note that transforms near Marion Island are not shown with the proper offsets to emphasize how a large-offset transform offsets the lithosphere and blocks sub-axial asthenospheric flow⁴⁸. Right side of the cartoon illustrates the Atlantis

Bank oceanic core complex, which is shown on the front face of the diagram, though its actual position (indicated by arrow) is to the north, flanking the transform valley. The ridge section between 53° E and 56° E with several oblique amagmatic rifts⁴⁹ is not shown.

thermal anomaly, mantle density variations seem to be the only possible explanation. The SWIR formed with the breakup of Gondwanaland about 180 million years ago, and the asthenosphere beneath the ridge was drawn up from beneath southern Africa, Madagascar and Antarctica. Therefore, it probably represents the depleted source mantle for the Karoo, Madagascar, and Ferrar flood basalt events emplaced into the asthenosphere. If this mantle represents compositionally buoyant mantle plumes, the depletion may go back even further in Earth history.

The other major rifted rise—the Azores Rise—is similar to the Marion Rise. It has only a 95-km-long axial high at its crest, and a deep axial rift along the rest of its 2,900-km length. Despite a focus on the neovolcanic zone, as at the Marion Rise, almost accidental sampling has found peridotites exposed at numerous locations up its length (Supplementary Fig. 3). In conclusion, then, there are two classes of rise: axial and rifted, one robustly magmatic, the other weakly so. Although their associated hotspots and tracks indicate related origins, the dramatic differences between them require explanation. We propose that, in general, the robustly magmatic axial rises are largely supported by present-day melting anomalies, and the weakly magmatic rifted rises are largely supported by mantle residues from the earlier history of the associated plumes.

METHODS SUMMARY

To interpret the crustal architecture along the SWIR, we collected as much detailed information on the proportions, state of alteration, tectonic and igneous fabrics, and primary igneous petrology of our rock samples as we could. This data was then used to identify the probable manner in which these samples were exposed to the sea floor, whether emplaced as large massifs by detachment faulting, or serpentine diapirism up high-angle faults that cut either vertically or laterally into mantle rock⁵⁰. We took particular care to exclude talc–serpentine and talc–tremolite schists and highly sheared serpentinites when assessing the proportion of mantle rocks collected from the sea floor that represent major basement outcrops.

Critical to our methodology are mantle and lower-crustal rocks exposed by detachment faults at oceanic spreading centres. These faults often operate for millions of years, exposing peridotite and gabbro on their footwalls, while the volcanic carapace spreads in the opposite direction. This produces oceanic core complexes that can expose many hundreds of square kilometres of plutonic rock on the sea floor, providing sections into the deep crust and upper mantle of regional significance. Their discovery and exploration over the past 20 years has revolutionized our understanding of crustal accretion at slow- and ultra-slow-spreading ocean ridges. A further development, which we discuss, is the discovery of large areas along the SWIR where there is little igneous crust, and mantle rock spreads onto the sea floor in both directions by extensional block

faulting at amagmatic accretionary ridge segments. Thus, interpretation of the data used here is a product of many years of exploration of plutonic rocks outcropping on the sea floor, as well as ocean drilling deep sections into lower crust and mantle massifs, which has led to an understanding of the mechanisms by which they are emplaced and their tectonic significance.

Full Methods and any associated references are available in the online version of the paper.

Received 30 September 2011; accepted 11 December 2012.

Published online 6 February 2013.

- Morgan, W. J. Deep mantle convection plumes and plate motions. *Am. Assoc. Petrol. Geol. Bull.* **56**, 203–213 (1972).
- Kincaid, C., Schilling, J.-G. & Gable, C. The dynamics of off-axis plume-ridge interaction in the uppermost mantle. *Earth Planet. Sci. Lett.* **137**, 29–43 (1996).
- Weir, R. W. *et al.* Crustal structure of the northern Reykjanes Ridge and Reykjanes Peninsula, southwest Iceland. *J. Geophys. Res.* **106**, 6347–6368 (2001).
- Ito, G. & Behn, M. D. Magmatic and tectonic extension at mid-ocean ridges: 2. Origin of axial morphology. *Geochem. Geophys. Geosyst.* **9**, Q09O12, doi:10.1029/2008GC001970 (2008).
- Wang, T., Lin, J., Tucholke, B. & Chen, Y. J. Crustal thickness anomalies in the North Atlantic Ocean basin from gravity analysis. *Geochem. Geophys. Geosyst.* **12**, Q0AE02, doi:10.1029/2010GC003402 (2011).
- Canales, J. P., Ito, G., Detrick, R. S. & Sinton, J. Crustal thickness along the western Galapagos Spreading Center and the compensation of the Galapagos hotspot swell. *Earth Planet. Sci. Lett.* **203**, 311–327, doi:10.1016/S0012-821X(02)00843-9 (2002).
- Cannat, M., Rommevaux-Jestin, C., Sauter, D., Deplus, C. & Mendel, V. Formation of the axial relief at the very slow spreading Southwest Indian Ridge (49° to 69° E). *J. Geophys. Res.* **104**, 22825–22843 (1999).
- Dick, H. J. B., Fisher, R. L. & Bryan, W. B. Mineralogic variability of the uppermost mantle along mid-ocean ridges. *Earth Planet. Sci. Lett.* **69**, 88–106 (1984).
- Georgen, J. E., Lin, J. & Dick, H. J. B. Models of mantle upwelling beneath the Southwest Indian Ridge: the effects of ridge-transform geometry on magma supply at an ultra-slow spreading ridge. *Eos* **79**, abstr. 854 (1998).
- Niu, Y. & O'Hara, M. J. Global correlations of ocean ridge basalt chemistry with axial depth: a new perspective. *J. Petrol.* **49**, 633–664 (2008).
- O'Hara, M. J. Is there an Icelandic mantle plume? *Nature* **253**, 708–710 (1975).
- Presnall, D. C. & Helsley, C. E. Diapirism of depleted peridotite—a model for the origin of hot spots. *Phys. Earth Planet. Inter.* **29**, 148–160 (1982).
- Muller, M. R., Minshull, T. A. & White, R. S. Segmentation and melt supply at the Southwest Indian Ridge. *Geology* **27**, 867–870 (1999).
- Zhang, T., Lin, J. & Gao, J. Y. Interactions between hotspots and the Southwest Indian Ridge during the last 90 Ma: implications on the formation of oceanic plateaus and intra-plate seamounts. *Sci. China Earth Sci.* **54**, doi:10.1007/s11430-011-4219-9 (2011).
- Muller, M. R., Robinson, C. J., Minshull, T. A., White, R. S. & Bickle, M. J. Thin crust beneath ocean drilling program borehole 735B at the Southwest Indian Ridge? *Earth Planet. Sci. Lett.* **148**, 93–107 (1997).
- Cannat, M. *et al.* Modes of seafloor generation at a melt-poor ultraslow-spreading ridge. *Geology* **34**, 605–608 (2006).

17. Jokat, W. *et al.* Geophysical evidence for reduced melt production on the super-slow Gakkel Ridge (Arctic Ocean). *Nature* **423**, 962–965 (2003).
18. Dick, H. J. B. *et al.* A long in-situ section of the lower ocean crust: results of ODP Leg 176 drilling at the Southwest Indian Ridge. *Earth Planet. Sci. Lett.* **179**, 31–51 (2000).
19. Dick, H. J. B., Tivey, M. A. & Tucholke, B. E. Plutonic foundation of a slow-spreading ridge segment: oceanic core complex at Kane Megamullion, 23°30'N, 45°20'W. *Geochem. Geophys. Geosyst.* **9**, 44, doi:10.1029/2007GC001645 (2008).
20. Klein, E. M. & Langmuir, C. H. Global correlations of ocean ridge basalt chemistry with axial depth and crustal thickness. *J. Geophys. Res.* **92**, 8089–8115 (1987).
21. Patriat, P. & Segoufin, J. Reconstruction of the Central Indian Ocean. *Tectonophysics* **155**, 211–234 (1988).
22. Sclater, J. G., Grindlay, N. R., Madsen, J. A. & Rommevaux-Jestin, C. Tectonic interpretation of the Andrew Bain transform fault: Southwest Indian Ocean. *Geochem. Geophys. Geosyst.* **6**, doi:10.1029/2005GC000951 (2005).
23. Duncan, R. A. Hot spots in the southern oceans—an absolute frame of reference for the motion of the Gondwana continents. *Tectonophysics* **74**, 29–42 (1981).
24. Georgen, J. E., Lin, J. & Dick, H. J. B. Evidence from gravity anomalies for interactions of the Marion and Bouvet hotspots with the Southwest Indian Ridge: effect of transform offsets. *Earth Planet. Sci. Lett.* **187**, 283–300 (2001).
25. Dick, H. J. B., Lin, J. & Schouten, H. An ultraslow-spreading class of ocean ridge. *Nature* **426**, 405–412 (2003).
26. Fisher, R. L. & Dick, H. J. B., Natland, J. & Meyer, P. S. Mafic/ultramafic suites of the slowly spreading Southwest Indian Ridge: PROTEA Exploration of the Antarctic Plate Boundary, 24°E–47°E. *Ophiolite* **11**, 147–178 (1986).
27. Le Roex, A. P., Dick, H. J. B. & Fisher, R. L. Petrology and geochemistry of MORB from 25°E to 46°E along the Southwest Indian Ridge: evidence for contrasting styles of mantle enrichment. *J. Petrol.* **30**, 947–986 (1989).
28. Dick, H. J. *et al.* How variable slow-spread ocean crust. *Eos* **84**, abstr. #V22F-01 (2003).
29. Dick, H. J. B. in *Magmatism in the Ocean Basins* (eds Saunders, A. D. & Norry, M. J.) 71–105 (Geological Society Special Publication No. 42, 1989).
30. Jaroslow, G. E., Hirth, G. & Dick, H. J. B. Abyssal peridotite mylonites: implications for grain-size sensitive flow and strain localization in the oceanic lithosphere. *Tectonophysics* **256**, 17–37 (1996).
31. Ildefonse, B. *et al.* Oceanic core complexes and crustal accretion at slow-spreading ridges. *Geology* **35**, 623–626 (2007).
32. Hellebrand, E., Snow, J. E., Dick, H. J. B. & Hofmann, H. Coupled major and trace-element indicators in mid-ocean ridge peridotites. *Nature* **410**, 677–681 (2001).
33. Sun, S.-s. Chemical composition and origin of the Earth's primitive mantle. *Geochim. Cosmochim. Acta* **46**, 179–192 (1982).
34. Dick, H. J., Tivey, M. A., Tucholke, B. E. & Cheadle, M. J. The plutonic foundation of a MAR ridge spreading segment: the Kane Oceanic Core Complex. *Eos* **86**, abstr. T33G-02 (2005).
35. Xu, M., Canales, J. P., Tucholke, B. E. & DuBois, D. L. Heterogeneous seismic velocity structure of the upper lithosphere at Kane oceanic core complex, Mid-Atlantic Ridge. *Geochem. Geophys. Geosyst.* **10**, doi:10.1029/2009GC002586 (2009).
36. Kelemen, P. B. *et al.* Drilling mantle peridotite along the Mid-Atlantic Ridge from 14° to 16°N. *Proc. ODP Init. Rep.* **209**, (Ocean Drilling Program, 2004).
37. Cannat, M. *et al.* Ultramafic and gabbroic exposures at the Mid-Atlantic Ridge: geologic mapping in the 15°N region. *Tectonophysics* **279**, 193–213 (1997).
38. Blackman, D. K. *et al.* *Proceedings of the Integrated ODP 304/305* (Integrated Ocean Drilling Program Management International, doi:10.2204/iodp.proc.304305.2006 (2006).
39. Morishita, T. *et al.* Igneous, alteration and exhumation processes recorded in abyssal peridotites and related fault rocks from an oceanic core complex along the Central Indian Ridge. *J. Petrol.* **50**, 1299–1325 (2009).
40. Teagle, D. A. *et al.* Drilling a complete in situ section of upper oceanic crust formed at a superfast spreading rate: hole 1256D. *Eos* **87** (52), abstr. B31B-1090 (2006).
41. Cannat, M., Sauter, D., Escartin, J., Lavier, L. & Picazo, S. Oceanic corrugated surfaces and the strength of the axial lithosphere at slow spreading ridges. *Earth Planet. Sci. Lett.* **288**, 174–183 (2009).
42. Jordan, T. H. in *The Mantle Sample: Inclusions in Kimberlites and Other Volcanics* (*Proceedings of the Second International Kimberlite Conference*) (eds Boyd, F. R. & Meyer, H. O. A.) Vol. 2, 1–14 (American Geophysical Union, 1979).
43. Cadio, C., Ballmer, M. D., Panet, I., Diament, M. & Ribe, N. New constraints on the origin of the Hawaiian swell from wavelet analysis of the geoid to topography ratio. *Earth Planet. Sci. Lett.* **359–360**, 40–54, doi:org/10.1016/j.epsl.2012.10.006 (2012).
44. Ito, G., Shen, Y., Hirth, G. & Wolfe, C. J. Mantle flow, melting, and dehydration of the Iceland mantle plume. *Earth Planet. Sci. Lett.* **165**, 81–96 (1999).
45. Detrick, R. S., Needham, H. D. & Renard, V. Gravity anomalies and crustal thickness variations along the Mid-Atlantic Ridge between 33°N and 40°N. *J. Geophys. Res.* **100**, 3767–3787 (1995).
46. Canales, J. P., Detrick, R. S., Lin, J., Collins, J. A. & Toomey, D. R. Crustal and upper mantle seismic structure beneath the rift mountains and across a non-transform offset at the Mid-Atlantic Ridge. *J. Geophys. Res.* **105**, 2699–2720 (2000).
47. Karson, J. A. *et al.* Detachment shear zone of the Atlantis Massif core complex, Mid-Atlantic Ridge, 30°N. *Geochem. Geophys. Geosyst.* **7**, Q06016, doi:10.1029/2005GC001109 (2006).
48. Georgen, J. E. & Lin, J. Plume-transform interactions at ultra-slow spreading rates: Implications for the Southwest Indian Ridge. *Geochem. Geophys. Geosyst.* **4** (9), 9106, doi:10.1029/2003GC000542 (2003).
49. Dick, H. J., Lin, J., Michael, P. J., Schouten, H. & Snow, J. E. Ultra-slow-spreading—a new class of ocean ridge. *Eos* **83**, abstr. T52E-05 (2002).
50. Dick, H. J. B., Arai, S., Hirth, G., John, B. J., KROO-06 Scientific Party. A subhorizontal cross-section through the crust mantle boundary at the SW Indian Ridge. *Geophys. Res. Abstr.* **3**, 794 (2001).

Supplementary Information is available in the online version of the paper.

Acknowledgements This work was supported by the Chinese National Key Basic Research Program (2012CB417300), China Ocean Mineral Resources Research and Development Association, and the US National Science Foundation (grant OCE-0526905). We thank the crew and scientists of RV *Dayang Yihao* Cruise 21. M. Sulanowska provided technical support. Z. Chen and Y. Liu analysed chrome spinels for us at the Guangzhou Institute of Geochemistry, Chinese Academy of Sciences. A glass sample from 53°E was analysed by F. Ji at the State Key Laboratory for Mineral Deposits Research, Nanjing University. We thank the Core and Rock Storage Facility of the Woods Hole Oceanographic Institution for curatorial support and access to samples. D. Sauter, R. Fisher and E. Bonatti provided additional unpublished sample descriptions and locations for the eastern and western SWIR. A review by Y. Niu encouraged us to provide more appropriate measurements of ridge depth and directed us to several important papers, greatly benefiting the manuscript and its conclusions.

Author Contributions This article represents the first report of results of a survey during Cruise 21 Leg 5 of the RV *Dayang Yihao* directed by H.Z., who also had additional analytical work done at his institution. H.J.B.D. collected the bulk of the sample data over a period of 35 years. Both authors interpreted the results, with H.J.B.D. primarily responsible for the written text.

Author Information Reprints and permissions information is available at www.nature.com/reprints. The authors declare no competing financial interests. Readers are welcome to comment on the online version of the paper. Correspondence and requests for materials should be addressed to H.J.B.D. (hdick@whoi.edu) or H.Z. (zhouhy@tongji.edu.cn).

METHODS

The interpretation of crustal and upper mantle structure and architecture using seafloor samples is based on an understanding of the physical features of the samples: their igneous, metamorphic and structural characteristics, the tectonic setting in which they were collected, and the local seafloor physiography. Major features, such as detachment faults, high-angle normal faults, and transform walls provide exposures of the lower crust and mantle that can easily be misinterpreted. Here we summarize many of the key characteristics that guided our interpretation of the samples collected along the SWIR.

Although they comprise a relatively small proportion of mantle-derived rocks sampled along the SWIR, talc–tremolite and talc–serpentine schists can result in misinterpretation of basement lithology. Such schists represent a small percentage of SW Indian Ridge peridotites, certainly less than 10% (Supplementary Fig. 1), but accounting for these is important to our methodology for interpreting crustal architecture. Before the Integrated Ocean Drilling Program drilling at the Atlantis massif, the presence of such rocks suggested that the basement there was massive peridotite. However, 1,400 m, largely of gabbro, was drilled instead. Evidently the schists and included mylonite fragments found on the massif⁴⁷ were intruded along the detachment fault from where it cut peridotite emplaced in the transform domain to where it rooted in gabbro. These schists also occur *in situ* at Atlantis Bank⁵⁰, lying on 850 m of massive gabbro outcrop, and at Kane Megamullion on the MAR as fault gouge on statically altered massive peridotite and dynamically deformed gabbro¹⁹. They represent skins several metres thick, originally intruded along, and then exposed on, the footwalls of detachment faults, and are excluded in our interpretation of crustal architecture along the SWIR.

Another important consideration is serpentine diapirism up high-angle normal faults that cut into mantle rock at depth. This is seen in the Klamath Mountains of the western USA, where peridotite hydrated to serpentinite (studied by H.J.B.D.) is emplaced diapirically along high-angle faults that cut vertically or laterally into peridotite. This produces serpentinite belts up to hundreds of metres wide extending up to many tens of kilometres between unrelated metavolcanics and greywackes. They are highly deformed and sheared, often with facoidal peridotite blocks preserving primary granular textures. Missing are talc–serpentine schists, entrained mylonites, and any evidence of high-temperature faulting. This mode, representing late faulting and hydration of peridotite above the brittle–ductile transition, can account for the serpentinites in-faulted into lavas and gabbros in several shallow Deep Sea Drilling Program⁵¹ and Ocean Drilling Program⁵² MAR holes on the Azores Rise. Consequently, while the occurrence of highly sheared serpentinites support the idea that the crust may be thin, they do not provide direct evidence that the crust is missing.

Critical to our methodology is mantle and lower crust interpreted as emplaced to the sea floor by detachment faults where these rocks spread in one direction as the volcanic carapace spreads in the other⁵³. These faults often operate for millions of

years^{54,55}, requiring enormous heave and throw, producing distinctive bathymetric terrain^{16,25,56}. Almost half the MAR sea floor from 12.5° N to 35° N formed by such asymmetric spreading⁵⁸. At ultraslow-spreading ridges, peridotite is also emplaced over large areas by more symmetric block faulting at amagmatic ridge segments where the lithosphere is too strong to sustain low-angle faults^{16,25,58,59}. The associated high-temperature mylonites show both these fault classes rooted at high temperatures in the brittle–ductile transition in the mantle. Dredging, diving and drilling have documented many such large mantle massifs, such as at the MAR from 14° N to 16° N (refs 36, 37, 60, 61), at the Kane Megamullion¹⁹, and on the SWIR^{25,62}, as we also report here for the SWIR at 53° E.

Thus, interpretation of the rock sample data used in this paper to decipher crustal architecture along the SWIR is a result of many years of exploration of plutonic rocks outcropping on the sea floor by dredging, submersible and remotely operated vehicle (ROV), as well as ocean drilling deep sections into lower-crust and mantle massifs, which has led to an understanding of the mechanisms by which they are emplaced.

51. Bougault, H. & Cande, S. C. 1. Background, objectives, and summary of principal results: Deep Sea Drilling Sites 556–564. *Init. Rep. DSDP* **82**, 5–16 (1985).
52. Aumento, F. & Melson, W. G. *Initial Reports of the Deep Sea Drilling Project* Vol. 37, 1008 (US Government Printing Office, 1977).
53. Dick, H. J. B., Bryan, W. B. & Thompson, G. Low-angle faulting and steady-state emplacement of plutonic rocks at ridge-transform intersections. *Eos* **62**, 406 (1981).
54. Tucholke, B. E. & Lin, J. A geological model for the structure of ridge segments in slow spreading ocean crust. *J. Geophys. Res.* **99**, 11937–11958 (1994).
55. Cann, J. R. *et al.* Corrugated slip surfaces formed at ridge–transform intersections on the Mid-Atlantic Ridge. *Nature* **385**, 329–332 (1997).
56. Smith, D. K., Cann, J. R. & Escartin, J. Widespread active detachment faulting and core complex formation near 13° N on the Mid-Atlantic Ridge. *Nature* **442**, 440–443 (2006).
57. Escartin, J. *et al.* Central role of detachment faults in accretion of slow-spreading oceanic lithosphere. *Nature* **455**, 790–794 (2008).
58. Michael, P. J. *et al.* Magmatic and amagmatic seafloor spreading at the slowest mid-ocean ridge: Gakkel Ridge, Arctic Ocean. *Nature* **423**, 956–961 (2003).
59. Sauter, D. *et al.* Focused magmatism versus amagmatic spreading along the ultraslow spreading Southwest Indian Ridge: evidence from TOBI side scan sonar imagery. *Geochem. Geophys. Geosyst.* **5**, doi:10.1029/2004GC000738 (2004).
60. MacLeod, C. J. *et al.* Life cycle of oceanic core complexes. *Earth Planet. Sci. Lett.* **287**, 333–344 (2009).
61. Schroeder, T. *et al.* Nonvolcanic seafloor spreading and corner-flow rotation accommodated by extensional faulting at 15° N on the Mid-Atlantic Ridge: a structural synthesis of ODP Leg 209. *Geochem. Geophys. Geosyst.* **8**, doi:10.1029/2006GC001567 (2007).
62. Standish, J. J., Dick, H. J. B., Michael, P. J., Melson, W. G. & O’Hearn, T. MORB generation beneath the ultraslow-spreading Southwest Indian Ridge (9°–25° E): major element chemistry and the importance of process versus source. *Geochem. Geophys. Geosyst.* **9**, Q05004, doi:10.1029/2008GC001959 (2008).